IEEE Photonics Journal
An IEEE Photonics Society Publication

Ultrahigh Resolution Multiplexed Fiber Bragg Grating Sensor for Crustal Strain Monitoring

Volume 4, Number 3, June 2012

Q. Liu, Member, IEEE
T. Tokunaga
K. Mogi
H. Matsui
H. F. Wang, Member, IEEE
T. Kato
Z. He, Senior Member, IEEE

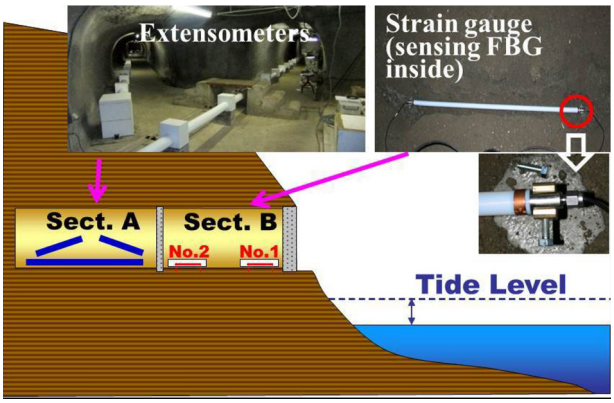

DOI: 10.1109/JPHOT.2012.2201217
1943-0655/$31.00 ©2012 IEEE

Ultrahigh Resolution Multiplexed Fiber Bragg Grating Sensor for Crustal Strain Monitoring

Q. Liu,[1] *Member, IEEE*, T. Tokunaga,[2] K. Mogi,[3] H. Matsui,[4] H. F. Wang,[5] *Member, IEEE*, T. Kato,[6] and Z. He,[1] *Senior Member, IEEE*

[1]Department of Electrical Engineering and Information Systems, The University of Tokyo, Tokyo 113-8656, Japan
[2]Department of Environment Systems, The University of Tokyo, Chiba 277-8563, Japan
[3]Department of Systems Innovation, The University of Tokyo, Tokyo 113-8656, Japan
[4]Geological Isolation Research and Development Directorate, Japan Atomic Energy Agency, Gifu 509-5102, Japan
[5]Department of Geoscience, University of Wisconsin-Madison, Madison, WI 53706 USA
[6]Earthquake Research Institute, The University of Tokyo, Tokyo 113-0032, Japan

DOI: 10.1109/JPHOT.2012.2201217

Manuscript received April 16, 2012; revised May 17, 2012; accepted May 18, 2012. Date of publication May 24, 2012; date of current version June 13, 2012. This research was sponsored by the Strategic International Cooperation Program from Japan Science and Technology Agency (JST), the Grant-in-Aid for Scientific Research (A) from Japan Science Promotion Society (JSPS), the Global Center of Excellence (G-COE) Program from the Ministry of Education, Culture, Sports, Science and Technology (MEXT), Japan. Corresponding author: Z. He (e-mail: zhe@ieee.org).

Abstract: We demonstrated a multiplexed fiber Bragg grating (FBG) sensor with static strain resolution of 10 nanostrain ($n\varepsilon$) for crustal strain monitoring. Each sensor unit consists of a pair of identical FBGs for strain sensing and reference, respectively. A narrow linewidth tunable laser is used to interrogate the FBGs, and a cross-correlation algorithm is incorporated to demodulate the wavelength difference induced by strain. When no strain is applied, an ultrahigh wavelength precision corresponding to strain resolution of 3.3 $n\varepsilon$ was obtained, indicating the ultimate resolution of the sensor system. With a variable strain applied by a piezo-stage, strain resolution of 17.6 $n\varepsilon$ was demonstrated. When the sensor is adopted for the in situ monitoring of crustal deformation, the strain induced by oceanic tide is clearly recorded with a resolution of 10 $n\varepsilon$, providing a potential tool for the geophysical measurements.

Index Terms: Sensors, fiber gratings.

1. Introduction

In geophysical research, the measurement of crustal deformation is of great relevance for studies of earthquakes and volcanoes [1], [2]. For those applications, strain sensors with a resolution on the order of nanostrain ($n\varepsilon$) in a static to low-frequency region are required. Conventional sensors for this purpose include extensometers and free-space laser interferometers. These sensors, however, are large in size, ranging from several tens to hundreds of meters in length, and thus difficult to be installed widely, especially in the deep underground. Moreover, because such a sensor can only give the integrated strain over its length, no spatially resolved deformation information can be obtained. On the other hand, fiber Bragg grating (FBG) strain sensors have well-known advantages such as small size, low cost, easy installation, high stability, and good linearity over a large strain range. They have already been widely adopted in applications like smart materials and structural

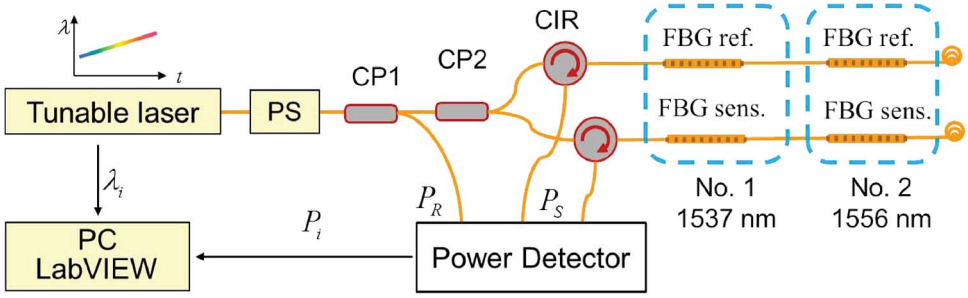

Fig. 1. Schematic of the FBG sensor system of in situ experiments. CP, coupler; CIR, circulator; PS, polarization scrambler.

health monitoring [3], and are also very attractive for geophysical applications if they can provide the required strain resolution. FBG sensors have realized even better than picostrain $(p\varepsilon)$ resolution in dynamic strain sensing [4]–[6], but their performance is not so satisfactory for static strain measurement. The dynamic strain signal like vibration repeats itself periodically, so it can be self-referenced. In contrast, the static strain signal rarely exhibits periodicity in the given time period, and the environmental interferences such as temperature change also falls into the static region. As a result, an extra reference has to be introduced in the static strain sensor, making it more complex than the dynamic sensor. The spectroscopic frequency associated with an atomic or molecular transition has been a popular reference for static strain sensing [7]–[9], but this type of reference cannot compensate for the drift of the sensor head due to environmental interference, and the narrow bandwidth of the transition also limits the measurement range of the sensor.

Recently we have developed a high resolution FBG static strain sensor with large measurement range for geophysical applications. The sensor consists of a pair of identical FBGs for reference and strain sensing, respectively. A narrow linewidth tunable laser is employed to interrogate the FBGs, and the Bragg wavelength difference between the two FBGs is extracted with a cross-correlation algorithm. When both FBGs were at relaxation without strain applied, an ultrahigh wavelength resolution corresponding to a static strain resolution of 3.3 $n\varepsilon$ was obtained, indicating the ultimate performance of the interrogation system. With a variable strain applied by a piezo-stage, strain resolution of 17.6 $n\varepsilon$ was demonstrated at laboratory. Then the sensor was adopted to measure the crustal deformation at Aburatsubo Bay, Japan. The strain induced by oceanic tide was clearly recorded with a resolution of 10 $n\varepsilon$, which is the first in situ demonstration of 10 $n\varepsilon$-order static strain resolution with FBG sensors, to the best of our knowledge.

2. Methodology

The configuration of the sensor system for crustal strain monitoring is schematically illustrated in Fig. 1. The sensor system has two sensor units interrogated by a narrow linewidth tunable laser using wavelength-division-multiplexing (WDM) technique.

2.1. Sensor Configuration

Each sensor unit consists of a pair of identical FBGs for sensing and reference, respectively. Although it is difficult to have FBGs with exactly the same parameters, the FBGs from the same batch can be regarded as identical. The sensor system works even the two FBGs have relatively large difference in nominal wavelength, spectral shape or temperature sensitivity, while the performance of the sensor will degrade accordingly. The sensing FBG is mounted on the measurand, and the reference FBG is strain-free, working as reference to distinguish the slow varying strain signal for the environmental disturbance like temperature drift which affect both the laser source and the sensor heads. The two FBGs are placed in close proximity so that they can have the same temperature. This condition is easy to satisfy in geophysical applications, because the sensor heads are usually installed in enclosed space underground with very stable environment temperature

(< 0.5 °C/year). The wavelength of the narrow linewidth tunable laser sweeps to interrogate the FBGs, and the reflected lightwaves are measured by high-sensitivity optical power detectors. About 10% of the power from the laser source is diverted by a coupler (CP1) as a power reference for ratio power detection to eliminate the source power variation during the wavelength sweeping. A polarization scrambler (PS) is employed to eliminate the influence of polarization instability.

For either sensor unit, strain information is obtained from the Bragg wavelength difference between the spectra of the sensing and the reference FBGs, so the sensor is immune to the long term wavelength drift of the laser. The two FBGs have the same nominal Bragg wavelength in order to eliminate the influence of wavelength nonlinearity during laser wavelength sweeping. The maximum reflection of the FBGs is chosen around 70%, considering both bell-shaped spectral profile and high reflection. According to the analysis on this type of sensor, FBGs with bell-shaped spectral profile is more suitable compared with high reflection FBGs [10].

2.2. Cross-Correlation Algorithm

While the wavelength of the tunable laser sweeps over the principal peaks of the FBGs' spectra, the reflectivity of FBGs are sampled as a discrete sequence of $R(\lambda_i)$ with a wavelength step of $d\lambda$. Considering one sensor unit, the reflectivity of the sensing FBG is labeled as $R_S(\lambda)$, while that of the reference FBG is labeled as $R_R(\lambda)$. Assuming that the two FBGs have the same spectral shapes when the sensing FBG experiences strain, the reflectivity satisfies

$$R_R(\lambda_i) = R_S(\lambda_i + \Delta\lambda) = R_S(\lambda_{i+\delta}) \tag{1}$$

where $\Delta\lambda$ is the wavelength shift caused by strain, and $\delta = \Delta\lambda/d\lambda$ is the corresponding index shift.

We use a cross-correlation algorithm to retrieve the Bragg wavelength difference $\Delta\lambda$ from the measured spectra, because of its advantage in suppressing random noise [10]. Once the spectra of the sensing and reference FBGs are recorded, their cross-correlation product is calculated as

$$C(j) = \sum_{i=-N}^{N} R_S(\lambda_{i+j}) R_R(\lambda_i) = \sum_{i=-N}^{N} R_S(\lambda_{i+j}) R_S(\lambda_{i+\delta}). \tag{2}$$

In (2), it is assumed that both $R_S(\lambda_i)$ and $R_R(\lambda_i)$ are equal to zero if the indices lie outside their ranges. This assumption is acceptable as long as the laser sweeping range covers the whole principal peaks of both FBGs. According to the properties of cross-correlation, $C(j)$ has the maximum when the two spectra overlap, i.e., $j = \delta$. Inversely δ can be demodulated from the index where $C(j)$ reaches its maximum. Due to the random errors in the measured spectra, the retrieved δ deviates from $\Delta\lambda/d\lambda$, and the deviation range determines the resolution of the sensor. It should be mentioned that although the index of maximum of $C(j)$ is an integer near δ, δ can be precisely calculated either by interpolation or by curve fitting around the maximum of $C(j)$.

Fig. 2 shows an example of calculating Bragg wavelength difference using the cross-correlation algorithm. Fig. 2(a) is a group of measured spectra of the FBGs used for crustal strain monitoring (sensor unit No. 1 in Fig. 1). The normalized cross-correlation curve is shown in Fig. 2(b). Parabolic curve fitting is implemented around the peak of the curve to determine the position of the maximum, which is exactly the Bragg wavelength difference between the two FBGs.

The cross-correlation algorithm is a weighted average in nature, where the high reflection part of spectrum has larger weight in the detection of Bragg wavelength difference, and the low reflection part has smaller weight. This algorithm achieves good balance between utilizing all the sampling data and suppressing the associated noises, and it is robust and tolerant of different shapes of FBGs' spectra.

3. Laboratory Validation

Before the FBG sensor system was put into practice, its performance was validated in the laboratory. The system configuration for validation was similar to that in Fig. 1, while only one pair of FBGs was used.

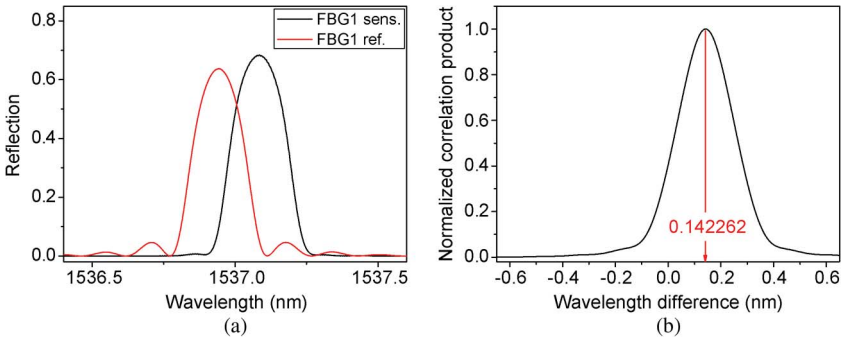

Fig. 2. Cross-correlation algorithm for Bragg wavelength difference calculation. (a) Measured spectra of FBGs of sensor unit No. 1 in Fig. 1. (b) The corresponding cross-correlation curve of the spectra. The Bragg wavelength difference is calculated to be 0.142262 nm.

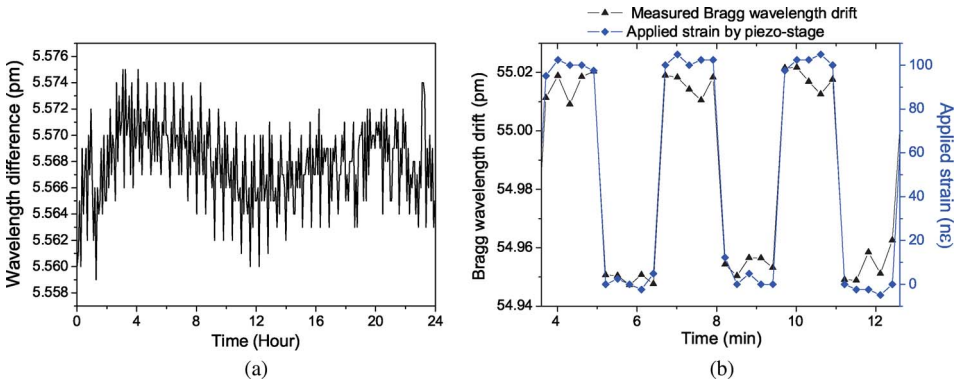

Fig. 3. Laboratory validation results. (a) Measured wavelength difference without strain applied. (b) Measured wavelength difference and applied strain. Diamond: Applied strain by the piezo-stage; Trigon: Measured Bragg wavelength difference between FBGs.

Laboratory validation was carried out without and with strain applied, respectively. First, both FBGs (fabricated by Fujikura Ltd.) were put in relaxation without strain applied to ascertain the ultimate resolution of the sensor system. A narrow linewidth tunable laser (Agilent 81680A, linewidth 100 kHz) was used to interrogate the FBGs with output power of about 0.1 mW, and the reflected lightwaves were measured by power detectors (Agilent 81634B). Both the laser and detectors are installed in a mainframe (Agilent 8164A), controlled by a personal computer (PC) via GPIB interface. The bandwidth (full width at 1/e maximum) of the FBGs was about 56 pm, and the laser wavelength sweeping range was 91 pm to cover the principal reflection peaks of FBGs. The laser wavelength was swept with a step of 0.1 pm, taking about 15 minutes to complete a sweep. The Bragg wavelength difference between the two FBGs was then calculated from the measured spectra after each sweep. The measured wavelength difference over 24 hour is shown in Fig. 3(a). The data fluctuate due to systemic noises and ambient interference, and this is the reason for the resolution limitation of the sensor system. The slow drift of curve is possibly caused by the tiny temperature difference between the two FBGs as the temperature increased by 1 °C during the experiment. The measured wavelength difference has a standard deviation of 3.1 fm over 24 hours, much smaller than the wavelength step of the tunable laser. The strain sensitivity of the FBG is tested to be 0.93 pm/$\mu\varepsilon$, so a static strain resolution of 3.3 nε is achievable with this interrogation system.

There are a couple of reasons for the sensor to achieve nε strain resolution (fm wavelength resolution) by using a wavelength sweep step of 0.1 pm. First, the obtained spectra of the FBGs in each measurement are formed by hundreds of independent samples of $R(\lambda_i)$ during the laser

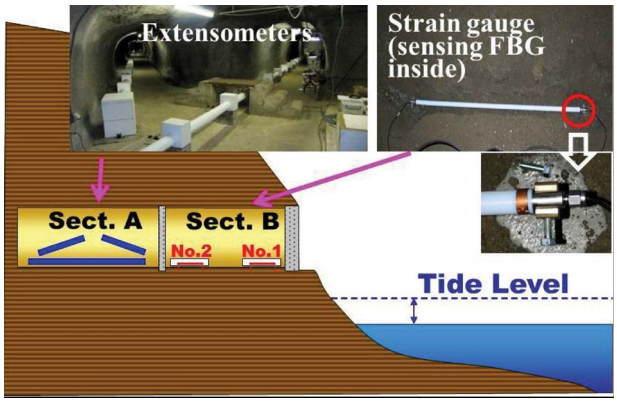

Fig. 4. Configuration for the measurement of crustal deformation induced by oceanic tide with extensometers and FBG sensors.

wavelength sweeping. Because the spectral profile of the FBG is smooth with bandwidth much larger than the wavelength step, the profile can be recovered exactly according to the Nyquist-Shannon sampling theorem, and then the peak of the profile can be determined with a resolution much better than the sampling interval, where interpolation or curve fitting can be used. Second, a cross-correlation algorithm is employed to calculate the Bragg wavelength difference directly from the measured data. The resolution of the FBG sensor is determined by the random errors in the measurement of wavelength λ_i and the corresponding reflection R. The cross-correlation algorithm has good ability in suppressing the associated noises with the obtained samples of $R(\lambda_i)$ to give a high wavelength (strain) resolution. A theoretical analysis on the resolution of this type of FBG sensors can be found in [10].

Then a piezo-stage (PI 752) was employed to supply a variable strain to the FBG sensor. The sensing FBG was mounted between a manual stage and the piezo-stage, and the reference FBG was mounted between two manual stages with a fixed strain. The laser and power detectors were the same as above, but the measuring period was reduced to several seconds by employing a continuous sweeping mode of the laser. A piezo-driver (PI E625) is employed to apply a switching strain to the sensing FBG with amplitude of 100 nε. At each strain level the measurement of the sensor system was repeated for 5 times with an interval of 20 s. A part of the measured data is shown in Fig. 3(b). The blue line is the applied strain by piezo-stage, calculated from the readout of the integrated displacement sensor in the piezo-stage. The black line is the measured Bragg wavelength difference between the FBGs, accurately following the applied strain change. At either applied strain level, the measured wavelength difference fluctuates due to the noise in the sensor system and ambient disturbance, and the strain resolution is calculated to be 17.6 nε over 5 h. The degradation of strain resolution was believed mainly limited by the instability of the piezo-stage.

4. Field Deployment

After the laboratory validation, the FBG sensor system was implemented to measure the crustal deformation at Aburatsubo Bay, at the tip of Miura Peninsula, Japan, which is about 60-km south-west of Tokyo and is surrounded by Pacific Ocean except on its northern side. As shown in Fig. 4, a vault was built on the coastline and situated under a cliff about 10-m high. As the oceanic tide level varies, the pressure of the water on the sea bed changes accordingly, resulting in a deformation of the rock mass. Silica tube extensometers with length of 38 m have been installed in Section A of the vault for strain measurement since 1976, which provide a comparison for our measurement with FBG sensors [11].

Two FBG sensor units (No. 1 and No. 2 in Fig. 1) were mounted inside Section B of the vault, as shown in Fig. 4. Each sensor unit consists of a commercially available FBG strain gauge (Micron Optics, os3600) and a reference FBG (fabricated by Fujikura Ltd.). Both of the 1-m long strain

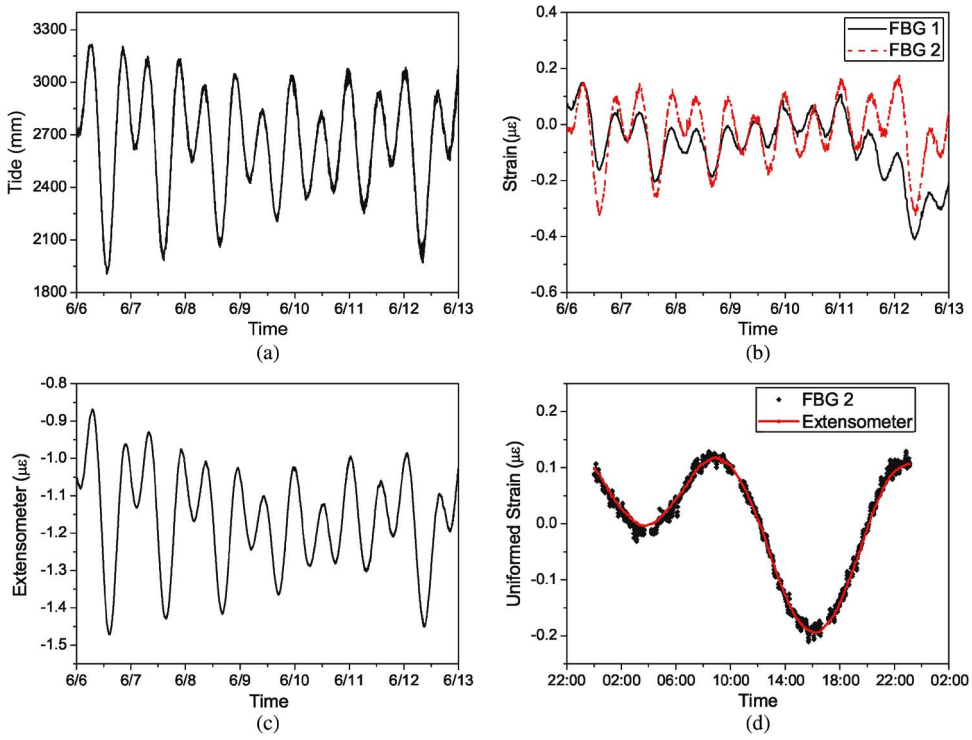

Fig. 5. In-situ experimental results during June 6–13, 2011. (a) Oceanic tide level. (b) Measured strain by FBG sensors. (c) Measured strain by an extensometer. (d) Comparison of measured strain given by extensometer and that by FBG No. 2 on June 8, 2011. The scale of the strain by extensometer is scaled by a factor of 0.76 and its offset is adjusted for comparison.

gauges were previously mounted between two steel anchors fixed about 30-cm deep into the rock bed. The nominal Bragg wavelengths are 1537 nm and 1556 nm for the two FBG strain gauges, respectively.

The developed FBG strain sensor has the best performance when the sensing and the reference FBGs have identical parameters, which is not a problem if the FBGs can be selected before experiments. In our field experiments, however, FBG strain gauges were previously installed, so we have to custom the reference FBGs according to the parameters of the existing sensing FBGs. The spectra of the sensing FBG and the customed reference FBG in sensor unit No. 1 are shown in Fig. 2(a). They have very similar spectral shape, and the tiny temperature sensitivity difference (10.1 pm/°C for the sensing FBG, 10.003 pm/°C for the reference FBG) is ignored in this experiment. A compensation on the difference of temperature sensitivity will further improve the performance of the FBG sensor, especially the long term stability.

The spectra of all the four FBGs have smooth spectra shape with bandwidth of 0.22 ± 0.02 nm, broader than that of the FBGs used in laboratory validation. According to the analysis on the performance of this type of FBG sensor [10], the resolution of this sensor system is mainly limited by the wavelength repeatability of the laser. FBGs with broader bandwidth work better to suppress the effect of wavelength repeatability, and can theoretically provide higher resolution.

The sensor configuration is the same as illustrated in Fig. 1. The distance between the two sensor units is 5 m, and the units are connected by 10-m long fibers. 25-m long fibers are used to connect the interrogation system and the first sensor unit. The interrogation system is in another sealed section of the vault, capable of continuous measurement for several months without maintenance. The narrow linewidth laser scans the two sensor units sequentially using WDM technique with a interval of 1 min. The long term stability of the sensor system is still under investigation, while the high static strain resolution has already been demonstrated. Parts of the in situ experimental results over one week (June 6–13, 2011) are shown in Fig. 5.

Fig. 5(a) and (b) illustrate the oceanic tide level and the measured strain by the FBG sensors, respectively. The measured strains by FBG sensors have similar shape to the oceanic tide level, showing that the oceanic-tide-induced crustal deformation is clearly observed. The different amplitudes between the two sets of FBG sensors in Fig. 5(b) probably reflect differences in deformation at the FBG mounting locations. If so, the results suggest the feasibility of measuring the distribution of rock mass deformation with high spatial resolution and low cost. Fig. 5(c) shows the data from the 38-m-long extensometer. Although the measured strain information is slightly different between the extensometer and the FBG sensors due to their different mounting spots and methods, we can use the data given by the extensometer to evaluate the resolution of the FBG sensors. Fig. 5(d) plots the comparison of the measured strain given by FBG No. 2 over a day and that by the extensometer for which the amplitude is scaled by a factor of 0.76 and the offset is adjusted for comparison. The measured strain by the FBG sensor fluctuates against that by the extensometer with a standard deviation of 9.8 nε. This is the first in situ static strain measurement of 10-nε order resolution with FBG sensors, to the best of our knowledge.

Compared with the extensometer, the FBG sensor has comparable strain resolution with much smaller size and lower cost. The small size not only reduces the difficulty and cost for mounting, but also making the quasi-distributed static strain measurement possible, especially the FBG sensors are good at multiplexed sensing. Better strain resolution is expectable if the sensing and reference FBGs are well matched in the following experiments. With the above characteristics, our FBG sensor shows a great potential for the geophysical applications.

5. Conclusion

In conclusion, we demonstrated a multiplexed FBG sensor system with a static strain resolution of 10 nε in geophysical measurements. A strain-free FBG identical to the FBG sensor head was used as the reference, enabling compensation of the drift from both the laser source and the sensor head. A cross-correlation algorithm was employed to extract the Bragg wavelength difference, i.e., the strain information, from the reflected spectral data of the FBGs, while suppressing the common random intensity and frequency noise and/or disturbance. With this sensor system at Aburatsubo Bay, Japan, the crustal deformation induced by oceanic tide is clearly observed with a static resolution of 10 nε, which is comparable with traditional extensometers of much larger size. This technique provides a potential tool for geophysical applications.

Acknowledgment

The authors thank Prof. K. Hotate at the University of Tokyo, Japan, for helpful discussions and comments. H. F. Wang acknowledges National Science Foundation (NSF) grant CMMI-0900351 and the Earthquake Research Institute for a three-month visiting professorship at the University of Tokyo.

References

[1] R. Bilham, R. Bendick, K. Larson, P. Mohr, J. Braun, S. Tesfaye, and L. Asfaw, "Secular and tidal strain across the main Ethiopian rift," *Geophys. Res. Lett.*, vol. 26, no. 18, pp. 2789–2792, Sep. 1999.

[2] P. Ferraro and G. De Natale, "On the possible use of optical fiber Bragg gratings as strain sensors for geodynamical monitoring," *Opt. Lasers Eng.*, vol. 37, no. 2/3, pp. 115–130, Feb./Mar. 2002.

[3] M. Majumder, T. K. Gangopadhyay, A. K. Chakraborty, K. Dasgupta, and D. K. Bhattacharya, "Fibre Bragg gratings in structural health monitoring—Present status and applications," *Sens. Actuators A, Phys.*, vol. 147, no. 1, pp. 150–164, Sep. 2008.

[4] B. Lissak, A. Arie, and M. Tur, "Highly sensitive dynamic strain measurements by locking lasers to fiber Bragg gratings," *Opt. Lett.*, vol. 23, no. 24, pp. 1930–1932, Dec. 1998.

[5] D. Gatti, G. Galzerano, D. Janner, S. Longhi, and P. Laporta, "Fiber strain sensor based on a pi-phase-shifted Bragg grating and the Pound-Drever-Hall technique," *Opt. Exp.*, vol. 16, no. 3, pp. 1945–1950, Feb. 2008.

[6] I. C. M. Littler, M. B. Gray, J. H. Chow, D. A. Shaddock, and D. E. McClelland, "Pico-strain multiplexed fiber optic sensor array operating down to infra-sonic frequencies," *Opt. Exp.*, vol. 17, no. 13, pp. 11 077–11 087, Jun. 2009.

[7] A. Arie, B. Lissak, and M. Tur, "Static fiber-Bragg grating strain sensing using frequency-locked lasers," *J. Lightw. Technol.*, vol. 17, no. 10, pp. 1849–1855, Oct. 1999.

[8] G. Gagliardi, M. Salza, P. Ferraro, and P. De Natale, "Fiber Bragg-grating strain sensor interrogation using laser radio-frequency modulation," *Opt. Exp.*, vol. 13, no. 7, pp. 2377–2384, Apr. 2005.
[9] T. T. Y. Lam, J. H. Chow, D. A. Shaddock, I. Littler, G. Gagliardi, M. B. Gray, and D. E. McClelland, "High-resolution absolute frequency referenced fiber optic sensor for quasi-static strain sensing," *Appl. Opt.*, vol. 49, no. 21, pp. 4029–4033, Jul. 2010.
[10] Q. Liu, T. Tokunaga, and Z. He, "Realization of nano static strain sensing with fiber Bragg gratings interrogated by narrow linewidth tunable lasers," *Opt. Exp.*, vol. 19, no. 21, pp. 20 214–20 223, Oct. 2011.
[11] K. Yamamura, O. Sano, H. Utada, Y. Takei, S. Nakao, and Y. Fukao, "Long-term observation of in situ seismic velocity and attenuation," *J. Geophys. Res.-Solid Earth*, vol. 108, no. B6, pp. 2317-1–2317-15, Jun. 2003.